Solar Wind Induced Waves in the Skies of Mars: Ionospheric Compression, Energization, and Escape Resulting From the Impact of Ultralow Frequency Magnetosonic Waves Generated Upstream of the Martian Bow Shock

Glyn Collinson, Lynn B. Wilson, Nick Omidi, David Sibeck, Jared Espley, Christopher M. Fowler, David Mitchell, Joseph Grebowsky, Christian Mazelle, Suranga Ruhunusiri, et al.

AGU100 ADVANCING EARTH AND SPACE SCIENCE

JGR

Journal of Geophysical Research: Space Physics

RESEARCH ARTICLE
10.1029/2018JA025414

This article is a companion to Fowler et al. (2018), https://doi.org/10.1029/2018JA025208.

Key Points:
- The impact of ultralow frequency (ULF) waves in the solar wind can drive compressional magnetosonic ULF waves in the ionosphere of Mars
- We survey MAVEN data, plus examine simultaneous multipoint observations by Mars Express, finding this phenomena occurs at Martian perihelion
- These ionospheric ULF waves drive compressive heating of the ionosphere and launch bursts of time-dispersed energetic ions

Correspondence to:
G. Collinson,
glyn.collinson@gmail.com

Citation:
Collinson, G., Wilson, L. B. III, Omidi, N., Sibeck, D., Espley, J., Fowler, C. M., et al. (2018). Solar wind induced waves in the skies of Mars: Ionospheric compression, energization, and escape resulting from the impact of ultralow frequency magnetosonic waves generated upstream of the Martian bow shock. *Journal of Geophysical Research: Space Physics*, *123*, 7241–7256. https://doi.org/10.1029/2018JA025414

Received 28 FEB 2018
Accepted 14 JUL 2018
Accepted article online 21 JUL 2018
Published online 28 SEP 2018

Solar Wind Induced Waves in the Skies of Mars: Ionospheric Compression, Energization, and Escape Resulting From the Impact of Ultralow Frequency Magnetosonic Waves Generated Upstream of the Martian Bow Shock

Glyn Collinson[1,2], Lynn B. Wilson III[1], Nick Omidi[3], David Sibeck[1], Jared Espley[1], Christopher M. Fowler[4], David Mitchell[5], Joseph Grebowsky[1], Christian Mazelle[6,7], Suranga Ruhunusiri[8], Jasper Halekas[8], Rudy Frahm[9], Tielong Zhang[10], Yoshifumi Futaana[11], and Bruce Jakosky[4]

[1]NASA Goddard Spaceflight Center, Greenbelt, MD, USA, [2]Institute for Astrophysics and Computational Sciences, The Catholic University of America, Washington, DC, USA, [3]Solana Scientific, Solana Beach, CA, USA, [4]Space Science Laboratory, University of California, Berkeley, CA, USA, [5]Space Sciences Laboratory, University of California, Berkeley, CA, USA, [6]L'Institut de Recherche en Astrophysique et Planétologie, CNRS, Toulouse, France, [7]University Paul Sabatier, Toulouse, France, [8]Department of Physics and Astronomy, The University of Iowa, Iowa City, IA, USA, [9]Southwest Research Institute, San Antonio, TX, USA, [10]Space Research Institute, Austrian Academy of Sciences, Vienna, Austria, [11]Swedish Institute of Space Physics, Kiruna, Sweden

Abstract Using data from the National Aeronautics and Space Administration *Mars Atmosphere and Voltatile EvolutioN* and the European Space Agency *Mars Express* spacecraft, we show that transient phenomena in the foreshock and solar wind can directly inject energy into the ionosphere of Mars. We demonstrate that the impact of compressive ultralow frequency waves in the solar wind on the induced magnetospheres drive compressional, linearly polarized, magnetosonic ultralow frequency waves in the ionosphere, and a localized electromagnetic "ringing" at the local proton gyrofrequency. The pulsations heat and energize ionospheric plasmas. A preliminary survey of events shows that no special upstream conditions are required in the interplanetary magnetic field or solar wind. Elevated ion densities and temperatures in the solar wind near to Mars are consistent with the presence of an additional population of Martian ions, leading to ion-ion instablities, associated wave-particle interactions, and heating of the solar wind. The phenomenon was found to be seasonal, occurring when Mars is near perihelion. Finally, we present simultaneous multipoint observations of the phenomenon, with the *Mars Express* observing the waves upstream, and Mars Atmosphere and Voltatile EvolutioN observing the response in the ionosphere. When these new observations are combined with decades of previous studies, they collectively provide strong evidence for a previously undemonstrated atmospheric loss process at unmagnetized planets: ionospheric escape driven by the direct impact of transient phenomena from the foreshock and solar wind.

1. Introduction

Without a global magnetic dipole field, the barrier to the solar wind at Mars and Venus is the conductive ionosphere. Interplanetary magnetic field (IMF) lines frozen into the solar wind flow collide with the ionosphere and pile up on the dayside, resulting in the generation of an induced magnetosphere. This induced magnetic field is an obstacle to the supersonic and super-Alfvénic solar wind, and thus, a supersonic and super-Alfvénic bow shock is generated (Ness et al., 1974; Russell et al., 1979). Just as at Earth, upstream of Mars (Brain, 2004; Grard et al., 1991; Mazelle et al., 2004; Russell et al., 1990) and Venus (Crawford et al., 1993a, 1993b, 1998; Orlowski & Russell, 1991) lies a region called the foreshock (Asbridge et al., 1968; Eastwood et al., 2005; Greenstadt et al., 1968). At Earth, the particles and waves in the foreshock generate and drive numerous transient phenomena which can have a global impact on our magnetosphere (Eastwood et al., 2008; Sibeck et al., 1998, 1999). Recent simulations by Omidi et al. (2017) show that, despite their diminutive size with respect to the ion gyroradius, the foreshocks of unmagnetized planets are nevertheless essentially identical to that at Earth, albeit in miniature. The foreshocks of Venus and Mars exhibit the same plethora of transient phenomena as at Earth, such as whistler waves (Brain et al., 2002; Orlowski & Russell, 1991), hot flow anomalies

(Collinson, Sibeck, et al., 2012, Collinson et al., 2014, 2015; Slavin et al., 2009), short large amplitude magnetic structures (Collinson, Wilson III, et al., 2012), and spontaneous hot flow anomalies (Collinson et al., 2017).

One phenomenon found upstream of all planetary bow shocks are ultralow frequency (ULF) electromagnetic waves, which are thought to be driven most efficiently by field-aligned ion beams reflected at the bow shock (Hoppe & Russell, 1983; Wilson, 2016) or produced locally (Ruhunusiri et al., 2016) from the pickup of ions from the geocorona of hot neutral hydrogen (Carruthers et al., 1976; Chaufray et al., 2008, 2012) and oxygen (Lichtenegger et al., 2009). At Earth, ULF waves are driven unstable by field-aligned ion beams through the ion/ion right-hand resonant instability (e.g., Wilson, 2016, and references therein). ULF waves have been observed ubiquitously upstream of both Mars and Venus (e.g., Brain et al., 2002; Crawford, 1995; Crawford et al., 1993a, 1993b; Delva & Dubinin, 1998; Delva et al., 2008; Dubinin & Fraenz, 2016; Dubinin et al., 2000; Fränz et al., 2017; Greenstadt, 1986; Wei et al., 2011). The intensity of ULF waves upstream of Mars (Halekas et al., 2017) and Venus (Delva et al., 2015) is strongly dependent upon the orientation of the interplanetary magnetic field, with more intense waves being observed when the IMF is *radial*, for example, parallel to the Sun-Planet line. At Mars, ULF waves exhibit a strong seasonal variation, with stronger waves closer to perihelion (Romanelli et al., 2016) due to the exospheric hydrogen that gets heated and enhanced at higher altitudes due to the brightening sunlight (Yamauchi et al., 2015). These waves attempt to propagate upstream (sunwards) but are blown backward toward the bow shock by the solar wind. As they approach the bow shock, they can "steepen" (Tsubouchi & Lembège, 2004; Wilson et al., 2009), roughly analogous to an ocean wave growing in height as it approaches the shoreline (although the underlying physics is completely different), becoming more oblique and compressional the deeper they go into the foreshock.

Magnetosonic ULF foreshock waves are thus packets of concentrated magnetic and plasma pressure that rain down upon a planetary bow shock. When they steepen and convect toward the shock, they can create their own localized wakes which affect the dynamic pressure locally exerted upon the bow shock, in some cases, creating strong enough wakes that they eventually become the new bow shock (e.g., Wilson, 2016, and references therein). It has been long known at Earth (Fairfield, 1976), and at Venus (Luhmann et al., 1983), that upstream pulsations and waves pass through the bow shock into the magnetosheath, especially at the *quasi-parallel* bow shock (Luhmann et al., 1987). At Earth, the magnetosphere mediates and absorbs much of the impact of foreshock processes (e.g., Eastwood et al., 2008; Russell et al., 1983; Sibeck et al., 1999; Sibeck et al., 1998). However, compressive ULF waves have been observed to penetrate Earth's magnetosphere (Du et al., 2010; Potapov & Polyushkina, 2010) and have been observed by ground stations in the Arctic and Antarctic (Du et al., 2010; Francia et al., 2012; Regi et al., 2014), albeit with only $\approx$5–10% of the wave energy than in the solar wind (Villante et al., 2011).

Unmagnetized planets such as Venus and Mars have no such protection: The boundary between the ionosphere and magnetosheath, the magnetopause, lies at the location where there is a sensitive balance between the internal pressure of the ionosphere and the total external pressure exerted by the shocked solar wind (Brace & Kliore, 1991; Brace et al., 1980; Martinecz et al., 2008; Russell et al., 1988). It has thus been hypothesized that foreshock processes may directly impart energy into the ionospheres of unmagnetized planets such as Venus and Mars (Collinson et al., 2015; Collinson, Sibeck, et al., 2012).

At Mars, solar wind plasma has been observed deep inside the magnetopause (Lundin et al., 2004), and compressive, linearly polarized ULF waves are frequently observed on both sides of the magnetopause (Bertucci et al., 2004), especially during solar storms (Espley et al., 2005). These results suggest that the magnetopause is far from an impenetrable shield to phenomena in the solar wind. Using ion and electron observations by the ESA *Mars Express*, Lundin et al. (2011) found electron fluctuations consistent with intense magnetosheath ULF waves entering the Martian ionosphere. They found a close correlation between solar wind dynamic pressure, ULF wave power, and O^+ outflow rates. Winningham et al. (2006) also reported electron pulsations in the Martian ionosphere observed by *Mars Express* with frequencies consistent with the typical O^+ gyrofrequency in the magnetosheath, further suggesting connectivity between waves in the sheath and the ionosphere. However, with no magnetometer aboard *Mars Express*, the magnetic fluctuations assumed to correspond with these plasma oscillations could not be confirmed, and their origin could not be investigated. Conversely, Espley et al. (2006) reported the observation of magnetic ULF waves in the Martian ionosphere by *Mars Global Surveyor* and suggested they may be due to "magnetosonic perturbations produced at higher altitudes in the Mars-solar wind interaction". However, the spacecraft carried no ion spectrometer and operated in a 400-km circular science orbit, so this could not be investigated. Recently, Halekas, McFadden, et al. (2015)

discovered and mapped bursts of time-dispersed energetic ions at Mars, with frequencies near the upstream proton cyclotron frequency, suggesting that upstream solar wind pressure perturbations may be a driver. Additionally, Fowler et al. (2017) found that electric field wave power, whose source was assumed to be within the magnetosheath, penetrates down to ~200-km altitude into the dayside upper ionosphere, further suggesting a non-Martian source of waves in the Martian ionosphere. Dubinin and Fraenz (2016) gave a recent overview of our current state of knowledge of ULF waves at Venus and Mars, clearly demonstrating connectivity between waves in the magnetosheath and ionosphere, speculating that ULF waves "take their origin in the foreshock/magnetosheath and then propagate to the ionosphere and further to the tail". Thus, whilst direct connectivity between solar wind/foreshock-driven processes directly impacting the ionopshere has been strongly suggested by decades of previous work, it has yet to be demonstrated experimentally.

Understanding how, and indeed *if*, waves in the solar wind can penetrate into the ionosphere of an unmagnetized planet is important, because it may have direct implications for our understanding of the physical processes that underly the evolution of the atmosphere and the dynamical interaction between the planetary magnetosphere/ionosphere system with the incident solar wind. Indeed, Ergun et al. (2006) argued that plasma waves, generated by the Mars-solar wind interaction might be a significant source of oxygen loss through heating of ionospheric particles. However, the evidence for this at the time was largely circumstantial, and thus, Ergun et al. (2006) strongly advocated for further observations.

Using in situ observations from the NASA *Mars Atmosphere and Voltatile EvolutioN (MAVEN)* Mars Scout, we show that the impact of compressive magnetosonic waves, from the upstream solar wind, drives linearly polarized, compressive magnetosonic waves in the ionosphere, inducing a localized "ringing" in the induced magnetosphere at the local proton cyclotron frequency. We show that these waves heat and compress the atmosphere and drive time-dispersed ions as hypothesized by Halekas, McFadden, et al. (2015), likely enhancing ion escape from the upper ionosphere as proposed by Ergun et al. (2006), Lundin et al. (2011), and Dubinin and Fraenz (2016). Expanding on this single case study to a preliminary survey of the phenomenon, we find that no special conditions are required in the interplanetary magnetic field or solar wind for waves upstream to drive compressive waves in the ionosphere. We also find that, consistent with a driven oscillator, the frequency of waves in the ionosphere linearly correlates with the frequency of waves upstream and in the solar wind. Additionally, we discover this to be a seasonal phenomenon, occurring when Mars is closest to the Sun (perihelion). Finally, we describe how a fortuitous alignment of the ESA *Mars Express* and the NASA *MAVEN* spacecraft enabled simultaneous multipoint observations of this phenomenon, with *Mars Express* acting as an upstream solar wind monitor and *MAVEN* observing the resulting driven ULF compression and "ringing" in the ionosphere.

A companion paper, Fowler et al. (2018), examines the impact of these ULF waves on the ionosphere of Mars in detail, finding that the magnetosonic waves drive large variations in ionospheric density and temperature and that the wave energy is absorbed by the dense ionosphere, leading to significant ion heating and substantial ion outflow.

2. Spacecraft Instrumentation

Here we present a brief overview of the instruments aboard the *MAVEN* and *Mars Express* spacecraft used for this study. Magnetic field data were measured by the *MAVEN* magnetometer (Connerney et al., 2015), consisting of two tri-axial fluxgate magnetometer sensors, with a resolution of 0.008 nT and a sample rate of 32 vector samples per second. Ion observations are presented from the *MAVEN* SupterThermal And Thermal Ion Composition (STATIC) instrument (McFadden et al., 2015), which measures ions over an energy range of 0.1 eV to 30 keV, a time resolution of 4 s, and with a 360° × 90° field of view and the ability to resolve H^+, He^{++}, He^+, O^+, O_2^+, and CO_2^+. Electron observations are presented from the *MAVEN* Solar Wind Electron Analyzer (SWEA; Mitchell et al., 2016), which has an energy range of 3–4,600 eV, a 360° × 120° field of view, and 2-s measurement cadence. Solar wind measurements are presented from the *MAVEN* Solar Wind Ion Analyzer (SWIA; Halekas, Taylor, et al., 2015), which measures ions over an energy range of 5 eV to 25 keV, and a 360° × 90° field of view. Additionally, this paper presents data from the *Mars Express* Analyzer of Space Plasmas and Energetic Atoms (ASPERA-3) Electron Spectrometer (ELS; Barabash et al., 2006), which measures electrons over an energy range of 0.01 to 20 keV, a 4-s time resolution, but a limited 2-D field of view (10° × 360°).

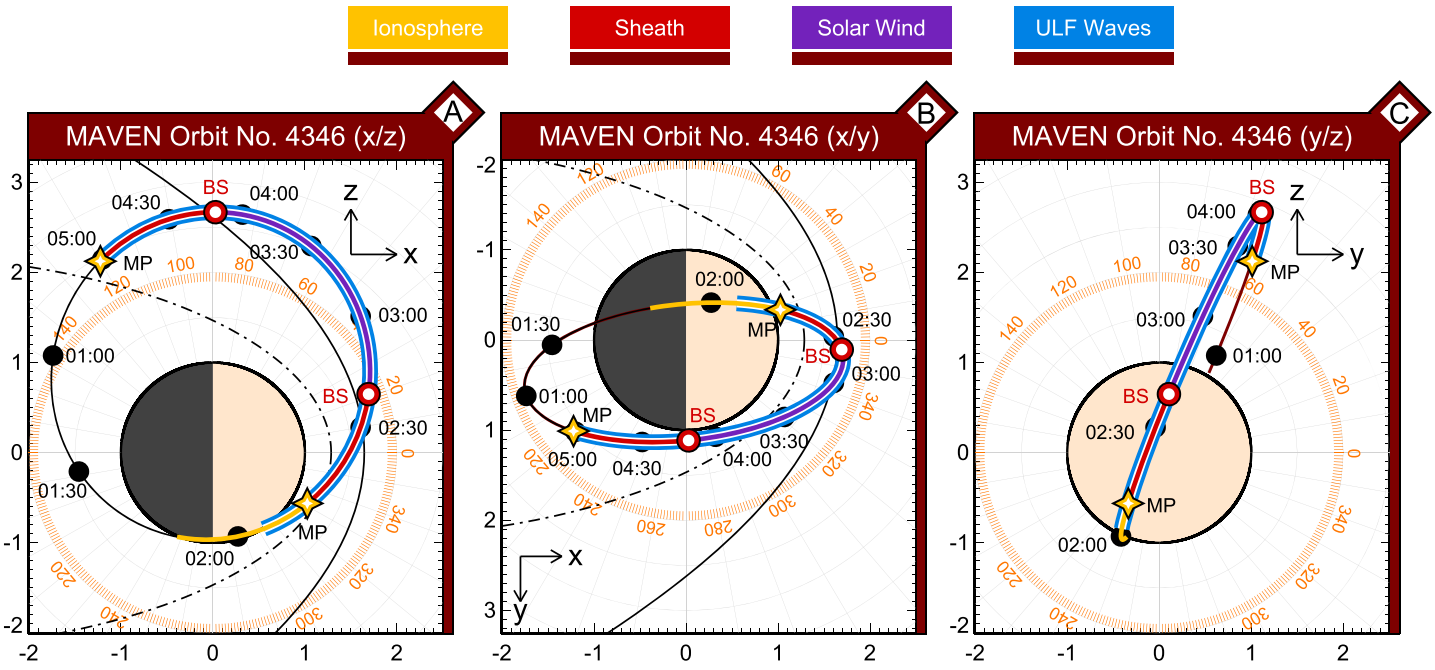

Figure 1. (a–c) Map of *MAVEN* orbit № 4346, with nominal bow shock (BS = solid black) and magnetopause (MP = dashed) according to Vignes et al. (2000). Units are in planetary radii, where $1R_M = 3,390$ km. *MAVEN* = Mars Atmosphere and Voltatile EvolutioN.

3. 25 December 2016: Foreshock-Driven ULF Waves in the Ionosphere of Mars

3.1. *MAVEN* Orbit № 4346

Figures 1a–1c shows a map of *MAVEN* orbit № 4346, occurring on Christmas Day, 25 December 2016. This paper uses the planet-centric Mars solar orbital coordinate system, where *X* points from the center of the planet towards the sun, *Y* points back along the tangent to the planet's orbit around the sun, and *Z* completes the right-handed system, pointing up out of the plane of the Martian ecliptic. Orbital maps show time intervals, average bow shock, and magnetopause positions and are color coded: Gold denotes passage through the ionosphere; red shows periods when the spacecraft was in the magnetosheath; and purple shows when the spacecraft was in the solar wind. Periods when ULF waves were observed are denoted in blue. *MAVEN* orbit № 4346 was a polar pass, inclined roughly along the Mars-Sun line, with periapsis over the south pole. *MAVEN* crossed the magnetopause into the magnetosheath at ≈02:11:30 Greenwich Mean Time (GMT) and crossed into the solar wind at ≈02:37:00 GMT. *MAVEN* then returned to Mars, crossing from the solar wind to the magnetosheath at ≈04:10:00 GMT and back through the magnetopause at ≈05:00:00 GMT. *MAVEN* observed ULF waves while in the ionosphere, in the magetosheath, and through the bow shock into the solar wind.

Figure 2 shows *MAVEN* magnetic field and particle observations from orbit № 4346: Figures 2a–2d show 50 min of data, covering passage from the ionosphere into the solar wind; Figures 2e–2h show a close-up of the magnetopause crossing, so that the ULF waves observed in the ionosphere may be better compared to those in the sheath. Figures 2a and 2e show a color-coded time line of the orbit (colors consistent with Figure 1). Figures 2b and 2f shows *MAVEN* Magnetometer data in Mars solar orbital coordinates, with magnetic field magnitude ($|B|$), three component magnetic field, and a wave-power spectrogram calculated using Morlet wavelet analysis (e.g., Torrence & Compo, 1998), where the *y* axis denotes the frequency of oscillations, and the color denotes the wave power at that frequency (in nT^2/Hz). Figures 2c and 2g show ion observations by the STATIC instrument (McFadden et al., 2015; time/energy spectrogram in differential energy flux $(cm^2 \cdot sr \cdot s \cdot eV)^{-1}$; plus density, temperature, and velocity of H^+, O^+, and O_2^+), and Figures 2d and 2h show electron observations by the SWEA (Mitchell et al., 2016; time/energy spectrogram in log_{10} counts per bin; plus electron density and temperature).

We shall now describe observations in each region in reverse order to which they were encountered (i.e., solar wind, magnetosheath, and ionosphere), because this makes the most logical sense for the scientific narrative, since the waves are forming upstream (Ruhunusiri et al., 2016) and transiting into the ionosphere and not vice versa.

3.2. Compressive Magnetosonic ULF Waves Form Upstream of Mars and Steepen as They Approach the Bow Shock

ULF waves were observed upstream of the Martian bow shock, consistent with previous observations of this phenomenon by Ruhunusiri et al. (2016) and recent statistical studies of compressive foreshock waves at Mars by Halekas et al. (2017). Using Minimum Variance Analysis, hodograms of the fluctuations in a field-aligned coordinate basis (Figure 3a) were found to exhibit an elliptical polarization. Consistent with these waves being compressive, magnetic field magnitude ($|B|$) and plasma density (both electrons and ions) oscillated in phase. Thus, we find that the waves were compressive in density and magnetic field with the magnetic field exhibiting elliptical polarization (the main components of the oscillation being the Bx and By components). Consistent with being fast/magnetosonic mode waves, they exhibit density and magnetic field magnitudes oscillating in phase, combined with a right-hand polarization with respect to the background field.

The majority of upstream ULF wave amplitudes exceeded 3 nT, well above the background 1.5-nT interplanetary magnetic field. As the waves approached the bow shock, their amplitudes steepened. In particular, two ULF waves (at 02:38:50 GMT and 02:39:25 GMT) had compression ratios $\left(\delta|B|/|B|_0\right) > 2$.

3.3. ULF Waves Steepen, Pile Up, and Form the Quasi-Parallel Bow Shock and Magnetosheath

As the ULF waves entered the magnetosheath, they strengthened and abruptly steepened further $\left(\delta B/B_0 = 6\right)$. Between 02:30 and 02:35 GMT, just inside the nominal location of the bow shock (Figure 1, 02:36:45 GMT, red circle), each wave crest rose to a mean |B| of 9.4 nT at the crests and returned to an IMF-like strength ($|B| = 1.6\ nT$) and orientation in each trough (Figure 2b). This is exactly as one would expect at the quasi-parallel bow shock, where each wavefront acts as its own localized quasi-parallel shock (Mann et al., 1994). As the amplitude of a wave increases, its phase speed also increases (Omidi & Winske, 1990). Thus, while still being blown backwards by the solar wind, these steepened waves can make more headway against the magnetosheath flow than their weaker siblings in the foreshock, and their velocity relative to the planet decreases. Just as at Earth, the result is that the waves pile-up and coalesce together to form the complex three-dimensional patchwork of the quasi-parallel shock and magnetosheath (Lucek et al., 2008; Schwartz & Burgess, 1991). The ULF waves had a frequency of ≈0.03 Hz (~30-s period) in both the foreshock and magnetosheath, near the upstream proton cyclotron frequency, indicated by a horizontal line in the wave power spectrogram (Figures 2b and 2f—dashed line at 0.03 Hz). Hodogram analysis of waves in the sheath (Figure 3b) show them to have retained their elliptical polarization.

3.4. Collision With the Magnetopause Driving Compressive Magnetosonic ULF Waves in the Ionosphere

As can be seen in the wave power spectrogram (Figure 2b), compressive ULF waves were observed continuously from the solar wind, through the magnetosheath, and into the ionosphere, with broadband wave emission observed at the magnetopause (Figure 2f). Using Minimum Variance Analysis, it was discovered that the polarization changes from circular near the bow shock to linear in the ionosphere (Figure 3c) and is transverse fast-mode waves. The frequency of oscillation increased slightly to 0.04 Hz (25 s) in the ionosphere, but there is nevertheless a clear continuum of the compressive wave activity in the solar wind and sheath. Two types of magnetic response are evident; the driven 0.03-Hz oscillation and a 2.5-s period localized "ringing" at the local proton cyclotron frequency (≈0.3 Hz, see thin black line in wavelet plot, Figure 2f). These local "ringing" waves, observed in the troughs of the ULF oscillations, are also linearly polarized magnetosonic-mode waves.

At Earth (Farrugia et al., 1989; Sibeck et al., 1989), Mercury, and Jupiter (Glassmeier et al., 2004), the impact of pressure pulsations in the solar wind is known to drive regular large-amplitude oscillations throughout the magnetospheric cavity and can result in electromagnetic "ringing" within the magnetosphere. At Mars, the polarization and frequency change between the sheath and ionosphere suggest that an analogous process may be occurring. In this instance, the waves are not directly penetrating into the ionosphere themselves. The sudden pulse of magnetic and plasma pressure associated with the impact of each wave crest on the magnetopause boundary is compressing the ionosphere and driving ULF waves within.

3.5. Impact on the Ionosphere

As with the magnetosonic waves in the sheath and solar wind/foreshock, the compressive ionospheric ULF waves drove density and temperature spikes in phase with the spikes in $|B|$ (Figures 2f–2h), consistent with plasma observations by Lundin et al. (2011) and magnetic observations by (Espley et al., 2006).

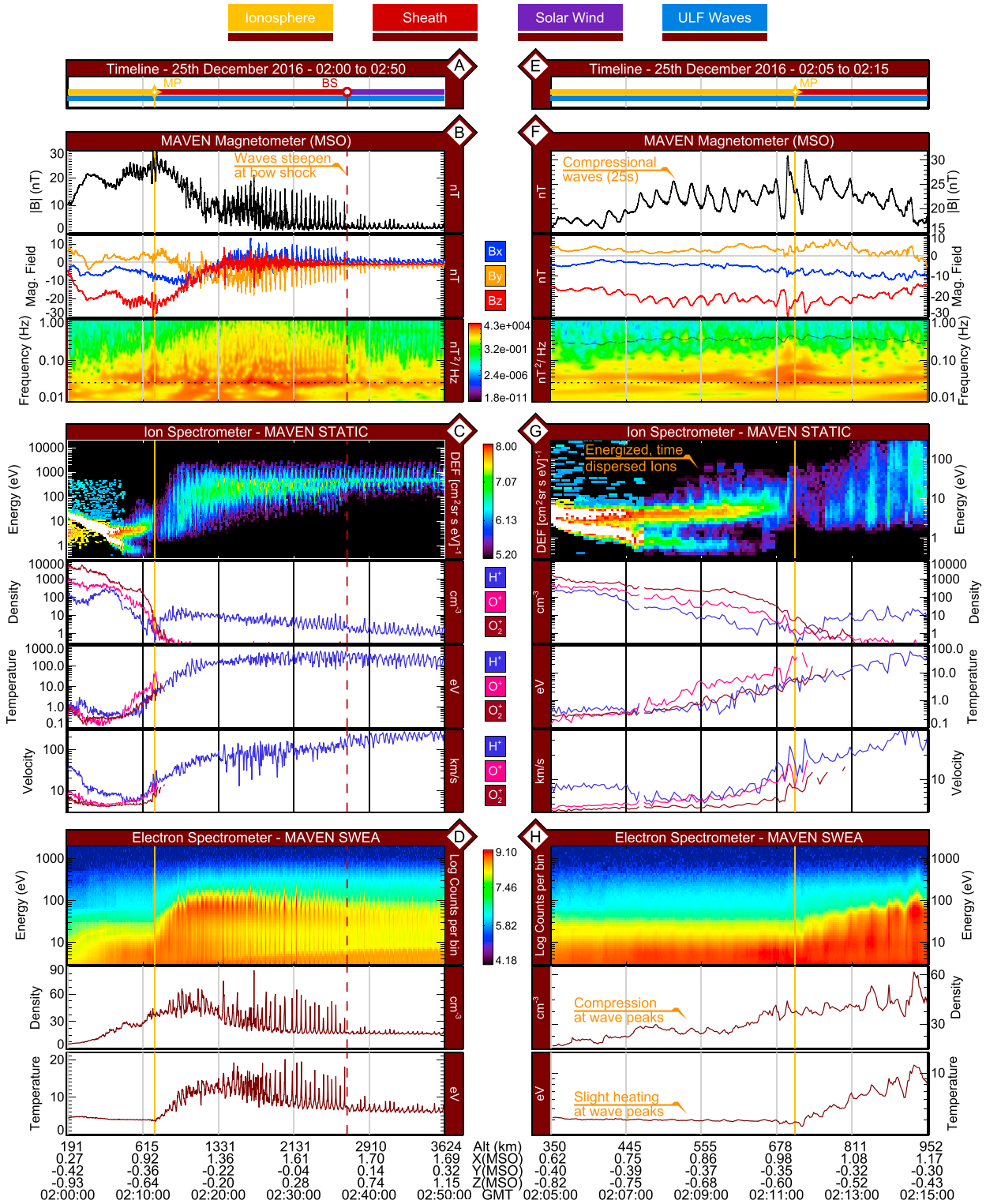

Figure 2. Penetration of upstream ULF waves into the ionosphere of Mars, observed by *MAVEN* on the 25 December 2016. (e)–(h) show 10 min of data to present a close-up of the magnetopause crossing; (a)–(d) show a longer (50 min) interval of data, showing the contiguous observation of ULF waves from the ionosphere into the solar wind. GMT = Greenwich Mean Time; *MAVEN* = Mars Atmosphere and Voltatile EvolutioN; MSO = Mars solar orbital; SWEA = Solar Wind Electron Analyzer; ULF = ultralow frequency.

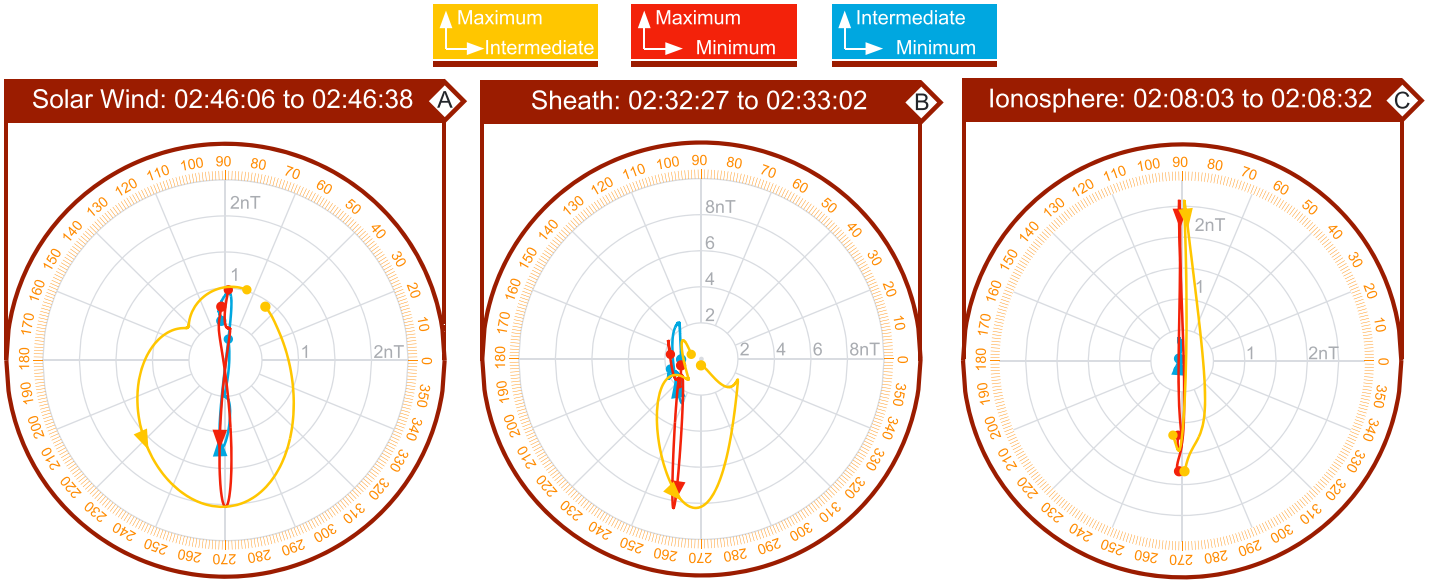

Figure 3. Hodograms of Mars Atmosphere and Voltatile EvolutioN magnetometer observations of waves: (a) ULF wave near the proton cyclotron frequency in the solar wind upstream of Mars showing circular polarization; (b) steepened ULF wave in the magnetosheath of Mars with circular polarization; and (c) ULF wave in the ionosphere of Mars showing linear polarization. Data have been passed through a low-pass (0.02 → 0.1 Hz) filter to remove the DC background field and higher frequency oscillations. ULF = ultralow frequency.

Furthermore, *MAVEN* STATIC observed in-phase velocity perturbations, together with energized, time-dispersed ions associated with the impact of each wave (Figure 2g, top panel). STATIC spectrograms in Figures 2c and 2g are limited to plotting a maximum flux of 10^8 $(cm^2 \cdot sr \cdot s \cdot eV)^{-1}$ to best show these dispersed signatures, which would otherwise be washed out by the very high fluxes associated with the core of the Martian ionosphere (white areas of the spectrogram). The bifurcation of the ion energy spectrogram is a result of different species, with the lower energy trace being associated with light ions (H^+) and the higher energy trace with heavier ions (O^+ and O_2^+). Such bursts of time-dispersed ions at close to the upstream proton cyclotron frequency are entirely consistent with those previously reported by Halekas, McFadden, et al. (2015) to occur globally and commonly. Halekas, McFadden, et al. (2015) hypothesized that such time-dispersed ions may be driven by the pressure pulses associated with low-frequency plasma waves generated upstream. The data presented here confirm this hypothesis.

The amplitude of the waves reduces from $\delta B/B_0 = 6$ in the sheath to $\delta B/B_0 = 1.15$ between the magnetopause and 450 km, further reducing to $\delta B/B_0 = 1.08$ below an altitude of 450 km and all but disappearing below ≈250-km altitude (02:03 GMT). One explanation for this damping is that it may be a result of the increase in background field strength. However, the correlation with signatures of plasma energization strongly suggests that this reduction in wave amplitude at lower altitudes is consistent with these waves being damped by the ionosphere. Thus, we find that these magnetosonic ULF waves in the ionosphere, induced by magnetosonic waves in the foreshock, are transferring their compressive energy into the ionosphere, in the form of heat and kinetic energy. Since all waves are below the ionospheric O^+ gyro-frequency, the primary mechanism the energization of ionospheric plasmas is unlikely to be through wave-particle resonances (although the local "ringing" waves will excite the local protons, a minor species). Rather, since heating occurs at the crest of each compressive ULF wave, we hypothesize that it is through compression and adiabatic heating that energy is being transferred between the ULF waves and the ionospheric plasma.

4. A Search for More Events

Expanding upon this initial case study, we searched for more events, examining 1,747 *MAVEN* orbits when the spacecraft reached apoapsis in the solar wind, spanning three periods:

1. 1 December 2014, orbit № 335, *Ls* 244° to 1 January 2015, orbit № 497, *Ls* 263°
2. 1 August 2014, orbit № 1632, *Ls* 21° to 1 December 2015, orbit № 2275, *Ls* 75°
3. 1 September 2016, orbit № 3750, *Ls* 214° to 1 March 2017, orbit № 4692, *Ls* 325°

Table 1
Upstream Conditions for Each Event (Waves Observed in Solar Wind, Sheath, and Ionosphere)

Orbit		IMF strength and angles			Solar wind conditions				Mars
		$\|B\|_{IMF}$	θ_{IMF}	$\theta_{\hat{B}.\hat{n}}$	n_{SW}	T_{SW}	V_{SW}	P_{SW}	*Ls*
№	Date	(nT)	(°)	(°)	(cm^{-3})	(eV)	(km/s)	(nPa)	(°)
335	01 December 2014	4.2	41.5	38.1	12.2	18.2	411	2.1	244
457	24 December 2014	4.5	23.5	57.0	9.2	10.0	362	1.1	258
481	28 December 2014	4.8	57.5	49.2	3.4	40.3	531	0.9	261
4193	25 November 2016	5.0	37.8	43.9	0.7	46.9	307	0.1	268
4214	29 November 2016	5.7	64.2	42.0	1.1	21.6	233	0.1	270
4219	30 November 2016	2.0	63.7	43.8	2.7	15.0	258	0.2	271
4346	25 December 2016	1.7	58.9	45.8	1.5	6.9	301	0.1	287
4353	26 December 2016	3.0	38.4	35.7	7.5	7.0	293	0.6	287
4372	29 December 2016	2.8	52.8	50.7	3.6	13.9	377	0.5	289
4403	29 December 2016	2.8	28.7	46.1	1.1	25.3	478	0.2	293
4415	07 January 2017	2.7	46.5	44.7	2.5	9.2	333	0.2	294
	Mean	3.6 nT	45.4°	45.2°	4.1 cm^{-3}	19.5 eV	353 km/s	0.55 nPa	275
	Standard dev.	±1.3	±15	±5.8	±3.8	±13.4	±91	±0.62	±16
	Typical	4*nT*	56°	-	2–3	4.8	408	0.6–0.8	-

Note. Interplanetary magnetic field (IMF) strength ($|B|$), cone angle (θ_{IMF}), and angle between IMF and bow shock normal vector ($\theta_{\hat{B}.\hat{n}}$) compared to typical Parker Spiral conditions at Mars; solar wind total density (n_{SW}), proton temperature (T_{SW}), proton velocity (V_{SW}), and dynamic pressure (P_{SW}) compared to typical conditions at Mars as measured by Mars Atmosphere and Voltatile EvolutioN (Halekas et al., 2017) and Martian solar longitude (*Ls*).

Out of these 1,747 orbits, ULF waves were observed to clearly occur continuously from the foreshock, sheath, and into the ionosphere during 11 orbits (including № 4346) or 0.63% of the time. Waves were observed in the ionosphere over a wide range of solar zenith angles (21.5° → 91.0°) but only on the day/upstream side. Waves were observed down to a minimum altitude of 186 km, although on average ULF waves were extinguished at a mean altitude of 412 ± 208 km.

4.1. Interplanetary Magnetic Field Conditions Were Typical

Table 1 shows conditions in the Interplanetary Magnetic Field (IMF) and solar wind during each event. First, we investigated the strength of the IMF ($|B|$) and the angle between the IMF and the Sun-Mars line (*cone* angle, θ_{IMF}). *MAVEN* magnetometer observations upstream were heavily smoothed to remove the distortions resulting from the waves and mean conditions taken over an average of 15 min of upstream observations. Halekas et al. (2017) found that the smaller the cone angle (i.e., the more radial the IMF, $\theta_{IMF} \approx 0°$), the stronger the ULF waves are upstream of Mars. Thus, our initial hypothesis was that these events would be confined to small cone angles. Suprisingly, however, the mean IMF cone angle during the events was 45.4° ± 15°, consistent with the typical Parker spiral angle of 56° at Mars (Parker, 1963). Similarly, foreshock-driven ionospheric ULF waves were observed over a wide range of IMF field strengths, with a mean (3.6 ± 4.2 nT) consistent with the ≈4 nT expected at Mars from a typical Parker-like expansion of the solar wind (Parker, 1965, 1958). Thus, these data do not suggest that any special conditions in the IMF are required for waves in the foreshock to excite ULF waves in the ionosphere.

4.2. All Occurred Near to Where the IMF was Normal to the Bow Shock

Next, we investigated the angle at which the IMF makes contact with the bow shock, by taking the mean IMF vector and extrapolating it in 3-D to where it makes contact with a Vignes et al. (2000) idealized Martian bow shock. At the location of IMF contact with the bow shock, the angle ($\theta_{\hat{B}.\hat{n}}$) was calculated between the IMF ($\hat{B}$) and the bow shock normal vector ($\hat{n}$). The values given in Table 1 together with the mean angle ($\theta_{\hat{B}.\hat{n}} = 45.2 \pm 5.8°$) should be considered a rough estimate, given the strong natural variability in the bow shock location (Mazelle et al., 2004), and that the type of ULF waves pervasive throughout these orbits is known to drive large motions in the bow shock (Omidi et al., 2017). However, our analysis suggests that the ULF waves were observed near to quasi-parallel conditions or, in other words, near to where the IMF was oriented normal to the surface of the bow shock. These conditions are known to be particularly conducive for the penetration of ULF waves from foreshock into the sheath (Luhmann et al., 1987), since at this location, the

Table 2
Properties of Waves Observed in the Solar Wind, Sheath, and Ionosphere

Orbit	Solar wind				Sheath				Ionosphere			
№	ω (Hz)	dB (nT)	$dB/\|B\|$	$\Theta_{\hat{k}.\hat{B}}$ (°)	ω (Hz)	dB (nT)	$dB/\|B\|$	$\Theta_{\hat{k}.\hat{B}}$ (°)	ω (Hz)	dB (nT)	$dB/\|B\|$	$\Theta_{\hat{k}.\hat{B}}$ (°)
335	0.080	0.33	0.08	22.7	0.063	4.57	0.48	86.2	0.063	0.47	0.011	76.9
457	0.073	0.32	0.07	16.6	0.073	2.42	0.22	76.0	0.073	0.25	0.008	54.4
481	0.036	1.21	0.25	33.7	0.068	2.69	0.17	70.6	0.068	0.73	0.029	86.2
4193	0.046	0.33	0.07	63.4	0.054	0.32	0.03	86.3	0.054	0.23	0.010	73.9
4214	0.031	0.39	0.07	36.3	0.029	0.37	0.05	83.0	0.029	0.19	0.008	71.9
4219	0.018	0.19	0.10	73.9	0.022	0.86	0.16	86.2	0.022	0.23	0.008	70.8
4346	0.027	0.17	0.10	33.4	0.038	0.36	0.08	88.7	0.038	0.17	0.009	73.3
4353	0.046	0.21	0.07	18.4	0.059	0.86	0.07	84.0	0.059	0.18	0.005	47.9
4372	0.056	0.16	0.06	24.2	0.054	1.57	0.27	74.9	0.054	0.27	0.005	79.9
4403	0.041	0.31	0.12	13.6	0.047	0.74	0.16	70.5	0.047	0.21	0.007	38.9
4415	0.042	0.26	0.09	15.3	0.044	1.01	0.14	73.7	0.044	0.19	0.006	15.0
Mean	0.04 Hz	0.35 nT	0.097	32.0°	0.05 Hz	1.43 nT	0.17	80.0°	0.05 Hz	0.21 nT	0.007	58.9°
	±0.02	±0.03	±0.05	±19	±0.02	±1.31	±0.12	±7	±0.016	±0.03	±0.002	±23

Note. Shown are frequency (Hz), absolute amplitude (nT), amplitude with respect to background field, and the angle between wave number and magnetic field ($\Theta_{\hat{k}.\hat{B}}$ in °).

IMF is stabbing down into the bow shock and providing magnetic connectivity for information (in the form of electromagnetic waves) to travel downstream.

However, one problem with this analysis is that although we are observing ULF waves in both the IMF and in the ionosphere, we are not making these observations along the same field line. By the time that *MAVEN* moves in to the ionosphere, it has traveled thousands of kilometers around Mars, and there is no way to know what angle the ionospheric field lines were originally oriented at to the bow shock, since the draping through the ionosphere has bent the field lines and this information has been lost. Thus, a proper investigation of the dependence on $\theta_{\hat{B}.\hat{n}}$ and the penetration of waves into the ionosphere will require future hybrid modeling studies.

4.3. The Solar Wind Was Hotter and Denser than Normal, Consistent With an Admixture of Martian Ions

Table 1 also shows mean upstream conditions in the solar wind for each event, as measured aboard *MAVEN* by the Solar Wind Analyzer (SWIA) instrument (Halekas, Taylor, et al., 2015). Shown are the total solar wind density (n_{SW} in cm^{-3}), proton temperature (T_{SW} in eV), velocity (V_{SW} in km/s), and total solar wind dynamic pressure (P_{SW} in nPa). At the bottom of the table are shown the mean and standard deviation of solar wind conditions from the 11 orbits, below which are typical conditions at Mars according to *MAVEN* SWIA observations by Halekas et al. (2017). Solar wind density and temperature were slightly elevated above normal. This is consistent with the presence of an additional population of ions (either fresh pickup or reflected ions from the bow shock), leading to ion-ion instabilities and associated wave-particle interactions (see, e.g., Ruhunusiri et al., 2016). Solar wind velocity and dynamic pressure were within normal limits. Thus, from these data, we posit: (a) The solar wind was contaminated with a secondary population of Martian ions, but (b) while measurement of the "clean" solar wind was not possible, there is no evidence to suggest any unusual conditions are required in the solar wind for waves in the foreshock to excite ULF waves in the ionosphere, beyond the presence of this admixture of Martian ions.

4.4. A Seasonal Effect, Occurring When Mars Is Near Perihelion

The final column of Table 1 shows the solar longitude (Ls) of the planet Mars during each orbit where waves in the foreshock were observed to drive ULF waves in the ionosphere. Without exception, all occurred near Southern Hemisphere Summer ($Ls = 275° \pm 16°$), when Mars is closest to the Sun (perihelion, Ls251). No events were observed during the second search period, occurring near to Martian aphelion. Of the 1,747 *MAVEN* orbits examined, only 583 occurred during this apparent southern summer wave season ($244 \leq Ls \leq 294$). When orbits outside of these range of Ls are disregarded, we find the probability of observing ionospheric wave excitation in this southern summer wave season was closer to ≈2%. However, this should

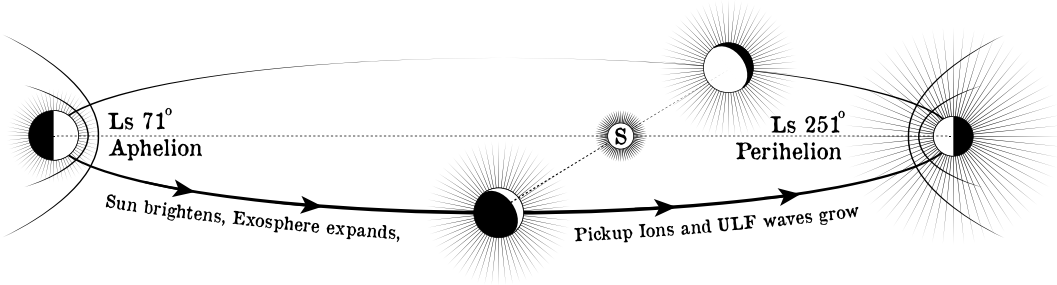

Figure 4. Sketch showing the evolution of Mars' hydrogen corona over the Martian year. *Ls* = solar longitude; ULF = ultralow frequency.

be considered a preliminary lower bound on how often ionospheric ULF wave excitation actually occurs, since the nature of our preliminary "by eye" search means that only events resulting in oscillations clearly visible to the eye were found. A more thorough analysis of how often this phenomenon occurs will require a more detailed statistical analysis and lies beyond the scope of this preliminary study.

Mars' orbit around the Sun is far more elliptical than Earth's (ϵ_{Mars} = 0.093 vs. ϵ_{Earth} = 0.017), and the resulting seasonal variations in the brightness of the Sun is known to drive global seasonal effects in the neutral atmosphere and foreshock. Yamauchi et al. (2015) found that pickup ions upstream from Mars are significantly enhanced around perihelion and suggested this was due to a seasonal enhancement in the underlying neutral exosphere. Romanelli et al. (2016) confirmed such a seasonal variation in the neutral exosphere, with neutral hydrogen densities (at altitudes of 3 Mars Radii) at perihelion ≈4× denser than at aphelion.

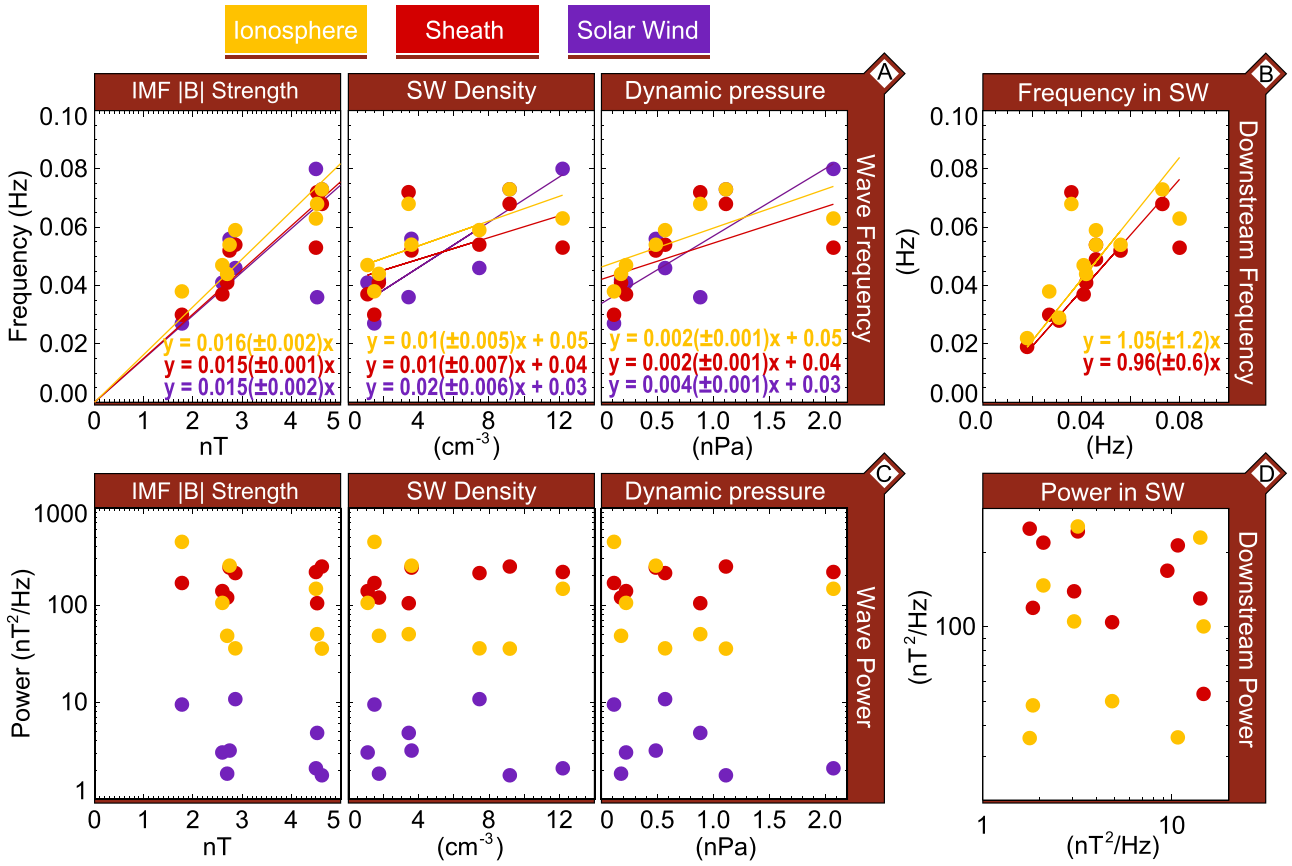

Figure 5. Plots showing the mean frequency (a and b) and power (c and d) of ultralow frequency waves in the ionosphere (gold), sheath (red), and solar wind ("SW" purple), in relation to mean upstream IMF and solar wind conditions (a and c), and to the frequency (b) and power (d) of waves in the three regions of the magnetosphere. Lines of linear best fit (using the least squares method) are overplotted for a and b. IMF = interplanetary magnetic field.

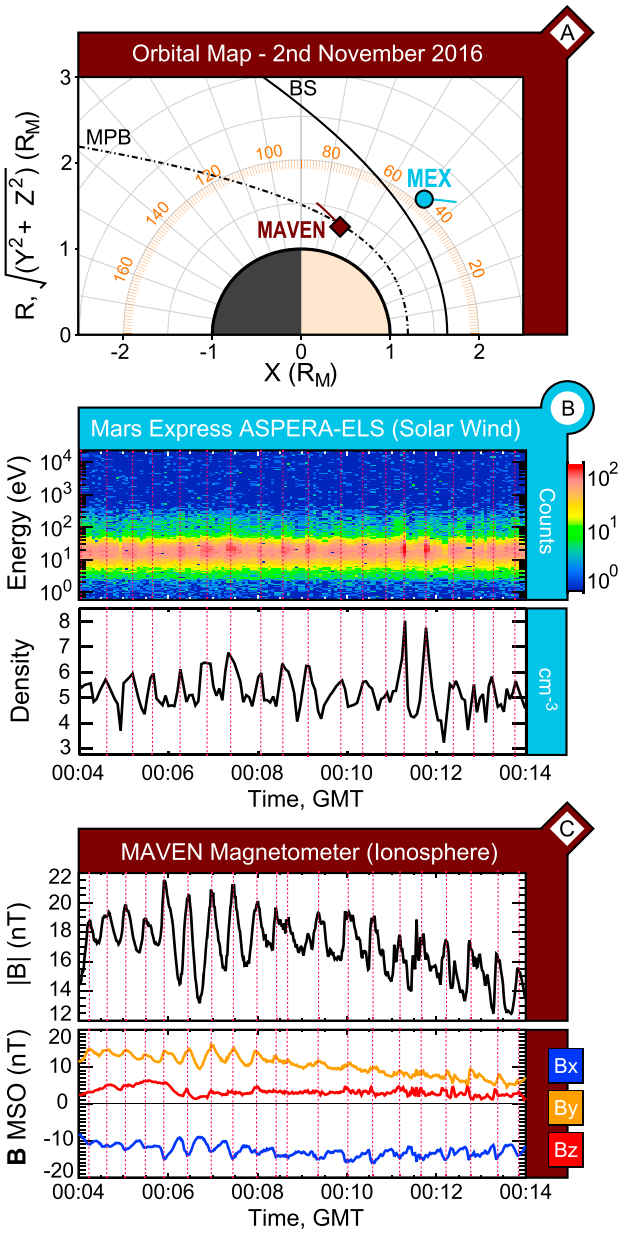

Figure 6. Simultaneous multipoint observations of ULF waves at Mars: (a) Map showing the locations of the *MAVEN* and *Mars Express* spacecraft with respect to nominal bow shock and magnetopause; (b) *Mars Express* ASPERA-ELS spectrogram and pseudo-density showing ULF waves in the foreshock of Mars; and (c) *MAVEN* Magnetometer observations of ULF magnetosonic waves in the ionosphere of Mars. ASPERA = Analyzer of Space Plasmas and Energetic Atoms; ELS = Electron Spectrometer; GMT = Greenwich Mean Time; MSO = Mars Solar Orbital; MAVEN = Mars Atmosphere and Voltatile EvolutioN; MEX = Mars Express; MPB = magnetopause boundary; ULF = ultralow frequency.

Romanelli et al. (2016) discovered that this coincided with a significant enhancement in the abundance of the ULF ("proton cyclotron") waves discussed in this study. Thus, our observations of foreshock-driven ULF waves in the ionosphere of Mars coincide with this known seasonal enhancement in the exosphere, in ion pickup, and in the abundance of proton cyclotron waves (see Figure 4).

4.5. The Properties of the Upstream ULF Waves Were Normal

Table 2 shows the properties of the ULF waves in the solar wind, sheath, and ionosphere; showing wave frequency (ω, in Hz), absolute amplitude (dB, in nT), ratio of amplitude with respect to the background field strength ($dB/|B|$), and the angle between wave number and magnetic field (°), where $\Theta_{\hat{k}.\hat{B}} = 90°$ is fully compressive. The frequencies given in Table 2 are the mean of a series of fits to a wavelet analysis and should only be considered in aggregate to obtain a general feel of their typical properties. As with our case study, all events exhibited continuous ULF waves at a quasi-constant frequency throughout the system. Curiously, the properties of ULF waves in the solar wind were within normal parameters according to the statistical study by Brain et al. (2002), and thus, there does not appear to be anything particularly "special" about them: they are the normal, compressive ULF waves, commonly observed upstream from Mars.

Consistent with our expectations, as these ULF waves pile up to form the quasi-parallel sheath, they steepen ($dB_{\text{Solar Wind}} = 0.35$ nT, $dB_{\text{sheath}} = 1.4$ nT) and become more compressive, with mean $\Theta_{\hat{k}.\hat{B}}$ increasing from $32° \pm 19°$ to $80° \pm 7°$. In the ionosphere, the waves were linearly polarized, compressive $\Theta_{\hat{k}.\hat{B}} = 59° \pm 23°$, with mean amplitude of 0.21 ± 0.03 nT.

4.6. Wave Frequency Is Conserved Throughout the System, Wave Power Is Not

Figure 5 shows scatter plots of wave frequency (Figures 5a and 5b) and power (Figures 5c and 5d) in the ionosphere (gold), sheath (red), and solar wind (purple).

4.6.1. Frequency

Figure 5b shows a plot of the frequency of ULF waves in the solar wind (x axis) on each orbit, compared to the frequency of waves observed downstream (y axis), showing a linear correlation. In other words, the higher the driving frequency in the solar wind and sheath, the higher the frequency of compressive waves in the ionosphere. This is as one would expect for a driven oscillator and provides further evidence that the waves in the ionosphere are being driven by the waves upstream. Figure 5a shows that the frequency of waves in the solar wind (and thus in the sheath and ionosphere) also linearly correlates with the strength of the IMF ($|B|$), as one would expect a wave at the cyclotron frequency to do. Interestingly, we observe that increasing solar wind density and dynamic pressure also correlate with increasing wave frequency.

4.6.2. Power

Figure 5d shows a plot of the power of the ULF waves in the solar wind (x axis) on each orbit, when compared to the power downstream. Unlike wave frequency, there is no clear correlation nor does wave power correlate with upstream properties (Figure 5c). We posit that this is a result of only being able to measure the wave power at a single point and is suggestive that local wave power is highly dependent on where the measurement is being made (as suggested by recent simulations of the Venusian foreshock by Omidi et al., 2017). Thus, it is not possible with a single spacecraft to accurately measure how much wave energy is being transported from the solar wind into the ionosphere but is a prime target for future simulations.

5. Simultaneous Multipoint Observations of Foreshock-Induced Ionospheric Waves at Mars

Finally, we present one additional but intriguing case study of foreshock-induced compression and localized "ringing" of the upper ionosphere of Mars. This event, occurred at a Martian solar longitude (*Ls*) of 253°, inside the southern summer wave season identified previously in section 4.4. At the time, the orbit of *MAVEN* was inclined such that it did not exit the bow shock and could not examine whether or not waves were present in the foreshock. Thus, while ULF oscillations were observed in the sheath, this event did not meet the stringent search criteria for our survey, requiring the unambiguous and continuous observation of waves by *MAVEN* in ionosphere, sheath, and solar wind. However, *MAVEN* is not the only spacecraft at Mars capable of measuring the solar wind.

Figure 6a shows the locations of *MAVEN* and *Mars Express* on 2 November 2016 with respect to nominal magnetopause boundary and bow shock locations. Between 00:04 and 00:14 GMT, *Mars Express* was in the solar wind, and *MAVEN* was in the topside ionosphere. Figure 6b shows an energy spectrogram from the *Mars Express* ASPERA-ELS instrument, together with a calculation of electron density (cm^{-3}). Note that due to the 2-D field of view of ASPERA-ELS, this has been calculated assuming isotropy and thus should be considered as pseudo-moment. Periodic ≈30-s enhancements in electrons were recorded, identical to those observed by *MAVEN* SWEA during the presence of compressive ULF magnetosonic waves (see, e.g., Figure 2d). Figure 6c shows simultaneous *MAVEN* magnetometer observations from the upper ionosphere, exhibiting the exact same response as all other events described in this paper: periodic ULF transverses oscillations near the driving frequency, and "ringing" in the troughs, with localized oscillations at the local proton cyclotron frequency.

These simultaneous multipoint observations provide additional strong evidence that these periodic ionospheric compressions are being driven by periodic pressure pulses in the solar wind.

6. Discussion and Conclusions

6.1. Foreshock-Driven Ionospheric Compression and "Ringing" at Mars

We show that transient phenomena in the foreshock and solar wind may directly impart energy into the ionosphere of an unmagnetized planet. As Mars approaches perihelion, the brightening sun heats the thermosphere, driving an expansion in the neutral hydrogen exosphere (Romanelli et al., 2016), which at Mars extends far beyond the bow shock and into the solar wind. At the same time, the brightening sun increases the rate of photoionization of the exosphere, resulting in an effectively bottomless source of protons upstream of Mars. The result is a significant enhancement in pickup ions upstream from Mars (Yamauchi et al., 2015). The presence of a second population of ions in the solar wind is a source of free energy for ULF waves to grow at the solar wind proton cyclotron frequency (see, e.g., Halekas et al., 2017; Ruhunusiri et al., 2016). These ULF foreshock waves, which are significantly more abundant around perihelion (Romanelli et al., 2016), steepen as they penetrate near the quasi-parallel bow shock. The impact of these compressive magnetosonic waves in the shocked solar wind with the magnetopause results in the generation of compressional, linearly polarized ULF magnetosonic waves in the ionosphere. These waves heat the ionosphere, energize ionospheric plasmas, and drive bursts of time-dispersed ions near the upstream proton cyclotron frequency. The change in frequency and polarization of the waves at the magnetopause suggests that the waves are not directly penetrating the ionosphere and that the ULF waves within are the result of a large-scale compression of the induced magnetosphere. Figure 7 shows a sketch of this phenomenon, based on simulations by Omidi et al. (2017).

Expanding on our initial case study, we performed a preliminary survey for more occasions when ULF oscillations were observed by *MAVEN* in the ionosphere, sheath, and solar wind. Eleven events were discovered, with foreshock-driven ULF waves observed in the ionosphere over a wide range of day/upstream-side solar zenith angles (21.5° → 91.0°), becoming damped below a mean altitude of 412 ± 208 km. Surprisingly, no unusual upstream conditions were required to observe foreshock-induced ULF waves in the ionosphere. The mean strength and orientation of the Interplanetary Magnetic Field (IMF) were consistent with what would be expected at Mars from a typical Parker Spiral. Mean solar wind velocity and dynamic pressure were consistent with typical conditions at Mars. Elevated solar wind densities and temperatures were consistent with the expected presence of an admixture of Martian ions, leading to ion-ion instablities, associated wave-particle interactions, and heating of the solar wind.

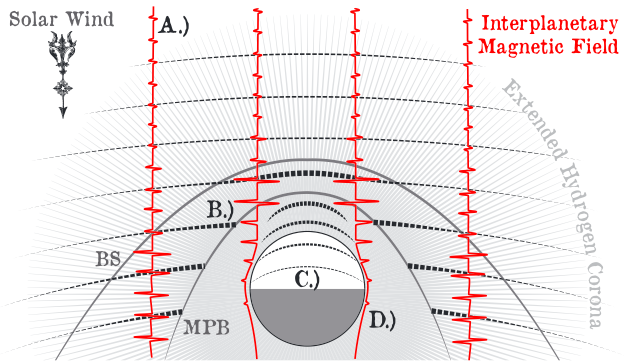

Figure 7. Sketch showing the penetration of upstream ULF waves through the magnetopause of Mars, resulting in ionospheric energization and escape. (a) ULF waves form upstream as a result of ion-ion instabilities; (b) ULF waves steepen and penetrate sheath; (c) The impact of each wave compresses the ionosphere driving ULF waves and localized "ringing"; (d) waves dampen, heating the ionosphere. ULF = ultralow frequency.

All events were confined to a narrow range of Martian solar longitude ($244 \leq Ls \leq 294$), consistent with this being a seasonal phenomenon occurring when Mars is closest to perihelion (at *Ls*251). Consistent with a driven oscillator, the frequency of ULF waves in the ionosphere was found to correlate with the frequency of waves in the solar wind and sheath. However, wave power was highly randomized, from which we posit that the strength of the waves is highly dependent on where they are being observed.

Finally, we presented simultaneous multipoint observations of this phenomenon at Mars, with the ESA *Mars Express* acting as an upstream solar wind monitor and the NASA *MAVEN* flying through the upper ionosphere. A periodic increase in counts was observed in the *Mars Express* ASPERA Electron Spectrometer identical to those resulting from compressive magnetosonic ULF waves. Near simultaneously, the *MAVEN* magnetometer observed magnetic signatures identical to the ionospheric compression and "ringing" observed on all other events presented here. These collected observations demonstrate beyond a reasonable doubt that the ULF activity in the ionosphere is a direct result of the impact of the pulses in pressure associated with the impact of each wave-crest in the solar wind.

6.2. The Impact on an Unprotected Ionosphere

Electromagnetic waves (including ULF waves) are known to play an important role in the energization and escape of ionospheric plasmas (e.g., Lundin et al., 2011; Strangeway, 1991, 2004). Consistent with this picture, we observe ionospheric compression and heating, demonstrating that foreshock-driven ionospheric waves impart thermal energy into the ionosphere. Velocity perturbations and time-dispersed ions were observed at each wave crest, demonstrating that, as hypothesized by Halekas, McFadden, et al. (2015), foreshock-driven ionospheric waves impart kinetic energy into ionospheric particles. Particle tracing simulations by Halekas, McFadden, et al. (2015) showed that the driving mechanism for these time-dispersed ion bursts is ion-pickup from the variable electric field in the wave. A companion paper by Fowler et al. (2018) examines the impact on the Martian ionosphere of this phenomenon in more detail. As with the event presented here, significant ion heating was observed all the way down to just above the exobase, likely caused by the damping of the magnetosonic wave by the dense ionosphere, and the density of the upper ionosphere was significantly lower when compared to preceding and following orbits of *MAVEN*, as if the upper ionosphere had been drained of plasma.

6.3. Foreshock-Driven Ionospheric Escape

We thus confirm the hypothesis that magnetic ULF waves in the ionosphere of Mars may be driven by ULF wave activity in the magnetosheath (Espley et al., 2004; Fowler et al., 2017; Lundin et al., 2011), which, in turn, may be formed by the steepening of compressive waves that are blown into the sheath from the quasi-parallel foreshock (e.g., Du et al., 2010; Lucek et al., 2008; Luhmann et al., 1983; Schwartz & Burgess, 1991). When these new observations are combined with the decades of past observations outlined in this paper (particularly Lundin et al., 2011, who found that ULF wave power closely correlated to O^+ outflow rates), they collectively provide strong evidence for a previously hypothesized (e.g., Collinson, Sibeck, et al., 2012; Dubinin & Fraenz, 2016; Lundin et al., 2011) atmospheric loss process at unmagnetized planets: ionospheric heating and escape driven directly by the impact of transient phenomena in the foreshock and solar wind. Such a mechanism has long been presumed to occur at Mars, and the observations presented here provide the missing link that finally and unambiguously connect ULF waves in the foreshock to those in the ionosphere.

While in this instance, the foreshock driver in question was periodic magnetosonic waves; it now seems even more plausible that pressure perturbations associated with other transient foreshock phenomena (such as hot flow anomalies, Collinson et al., 2014, 2015; and spontaneous hot flow anomalies, Collinson et al., 2017) will also impact the ionosphere.

Now that the direct link between foreshock phenomena and ionospheric perturbations have been demonstrated, this raises many more questions for the future: How common is foreshock-driven escape? What conditions are required for it to occur? Do foreshock-driven processes significantly enhance global ionospheric escape rates? How much energy is transported from the foreshock to the ionosphere? And, finally does this occur at all unmagnetized planets or only at Mars?

Acknowledgments
MAVEN data are available from the NASA Planetary Data System, and *MAVEN* data analysis software is freely available from the *MAVEN* Science Data Center (https://lasp.colorado.edu/maven/sdc/public/). This work was supported by NASA Solar System Workings Program grant NNX15A176G. At Southwest Research Institute, this work was supported under NASA contract NASW00003. We thank Mark Chaffin for useful discussions.

References

Asbridge, J. R., Bame, S. J., & Strong, I. B. (1968). Outward flow of protons from the Earth's bow shock. *Journal of Geophysical Research*, *73*, 5777–5782. https://doi.org/10.1029/JA073i017p05777

Barabash, S., Lundin, R., Andersson, H., Brinkfeldt, K., Grigoriev, A., Gunell, H., et al. (2006). The analyzer of space plasmas and energetic atoms (ASPERA-3) for the Mars Express mission. *Space Science Reviews*, *126*, 113–164.

Bertucci, C., Mazelle, C., Crider, D. H., Mitchell, D. L., Sauer, K., Acuña, M. H., et al. (2004). MGS MAG/ER observations at the magnetic pileup boundary of Mars: Draping enhancement and low frequency waves. *Advances in Space Research*, *33*, 1938–1944. https://doi.org/j.asr.2003.04.054, Comparative Magnetospheres.

Brace, L. H., & Kliore, A. J. (1991). The structure of the Venus ionosphere. *Space Science Reviews*, *55*, 81–163.

Brace, L. H., Theis, R. F., Hoegy, W. R., Wolfe, J. H., Mihalov, J. D., Russell, C. T., et al. (1980). The dynamic behavior of the Venus ionosphere in response to solar wind interactions. *Journal of Geophysical Research*, *85*, 7663–7678. https://doi.org/10.1029/JA085iA13p07663

Brain, D. A. (2004). The bow shocks and upstream waves of Venus and Mars. *Advances in Space Research*, *33*, 1913–1919. https://doi.org/10.1016/j.asr.2003.05.036

Brain, D. A., Bagenal, F., Acuña, M. H., Connerney, J. E. P., Crider, D. H., Mazelle, C., et al. (2002). Observations of low-frequency electromagnetic plasma waves upstream from the Martian shock. *Journal of Geophysical Research*, *107*, 1076. https://doi.org/10.1029/2000JA000416

Carruthers, G. R., Page, T., & Meier, R. R. (1976). Apollo 16 Lyman alpha imagery of the hydrogen geocorona. *Journal of Geophysical Research*, *81*(10), 1664–1672. https://doi.org/10.1029/JA081i010p01664

Chaufray, J., Bertaux, J., Leblanc, F., & Quémerais, E. (2008). Observation of the hydrogen corona with SPICAM on Mars Express. *Icarus*, *195*, 598–613. https://doi.org/10.1016/j.icarus.2008.01.009

Chaufray, J.-Y., Bertaux, J.-L., Quémerais, E., Villard, E., & Leblanc, F. (2012). Hydrogen density in the dayside Venusian exosphere derived from Lyman-α observations by SPICAV on Venus Express. *Icarus*, *217*, 767–778. https://doi.org/10.1016/j.icarus.2011.09.027, Advances in Venus Science.

Collinson, G. A., Sibeck, D. G., Masters, A., Shane, N., Slavin, J. A., Coates, A. J., et al. (2012). Hot flow anomalies at Venus. *Journal of Geophysical Research*, *117*, A04204. https://doi.org/10.1029/2011JA017277

Collinson, G., Halekas, J., Grebowsky, J., Connerny, J., Mitchell, D., Espley, J., et al. (2015). A hot flow anomaly at Mars. *Geophysical Research Letters*, *42*, 9121–9127. https://doi.org/10.1002/2015GL065079

Collinson, G. A., Sibeck, D. G., Masters, A., Shane, N., Zhang, T. L., Fedorev, A., et al. (2014). A survey of hot flow anomalies at Venus. *Journal of Geophysical Research: Space Physics*, *119*, 978–991. https://doi.org/10.1002/2013JA018863

Collinson, G., Sibeck, D., Omidi, N., Grebowsky, J., Halekas, J., Mitchell, D., et al. (2017). Spontaneous hot flow anomalies at Mars and Venus. *Journal of Geophysical Research: Space Physics*, *122*, 9910–9923. https://doi.org/10.1002/2017JA024196

Collinson, G. A., Wilson III, L. B., Sibeck, D. G., Shane, N., Zhang, T. L., Moore, T. E., et al. (2012). Short large-amplitude magnetic structures (SLAMS) at Venus. *Journal of Geophysical Research*, *117*, A10221. https://doi.org/10.1029/2012JA017838

Connerney, J., Espley, J., Lawton, P., Murphy, S., Odom, J., Oliversen, R., & Sheppard, D. (2015). The MAVEN magnetic field investigation. *Space Science Reviews*, 1–35. https://doi.org/10.1007/s11214-015-0169-4

Crawford, G. K. (1995). Comparison of upstream phenomena at Venus and Earth. *Advances in Space Research*, *16*. https://doi.org/10.1016/0273-1177(95)00219-5

Crawford, G. K., Strangeway, R. J., & Russell, C. T. (1993a). VLF imaging of the Venus foreshock. *Geophysical Research Letters*, *20*, 2801–2804. https://doi.org/10.1029/93GL01258

Crawford, G. K., Strangeway, R. J., & Russell, C. T. (1993b). VLF emissions in the Venus foreshock—Comparison with terrestrial observations. *Journal of Geophysical Research*, *98*, 15. https://doi.org/10.1029/93JA00634

Crawford, G. K., Strangeway, R. J., & Russell, C. T. (1998). Statistical imaging of the Venus foreshock using VLF wave emissions. *Journal of Geophysical Research*, *103*, 11,985–12,004. https://doi.org/10.1029/97JA02883

Delva, M., Bertucci, C., Volwerk, M., Lundin, R., Mazelle, C., & Romanelli, N. (2015). Upstream proton cyclotron waves at Venus near solar maximum. *Journal of Geophysical Research: Space Physics*, *120*, 344–354. https://doi.org/10.1002/2014JA020318

Delva, M., & Dubinin, E. (1998). Upstream ULF fluctuations near Mars. *Journal of Geophysical Research*, *103*, 317. https://doi.org/10.1029/97JA02501

Delva, M., Zhang, T. L., Volwerk, M., Magnes, W., Russell, C. T., & Wei, H. Y. (2008). First upstream proton cyclotron wave observations at Venus. *Geophysical Research Letters*, *35*, l03105. https://doi.org/10.1029/2007GL032594

Du, J., Zhang, T. L., Baumjohann, W., Wang, C., Volwerk, M., VöRöS, Z., & Guicking, L. (2010). Statistical study of low-frequency magnetic field fluctuations near Venus under the different interplanetary magnetic field orientations. *Journal of Geophysical Research*, *115*, A12251. https://doi.org/10.1029/2010JA015549

Dubinin, E., & Fraenz, M. (2016). Ultra-low-frequency waves at Venus and Mars. *Washington DC American Geophysical Union Geophysical Monograph Series*, *216*, 343–364. https://doi.org/10.1002/9781119055006.ch20

Dubinin, E., Sauer, K., Delva, M., Grard, R., Livi, S., Lundin, R., et al. (2000). Multi-instrument study of the upstream region near Mars: The Phobos 2 observations. *Journal of Geophysical Research*, *105*, 7557–7572. https://doi.org/10.1029/1999JA900400

Eastwood, J. P., Sibeck, D. G., Angelopoulos, V., Phan, T. D., Bale, S. D., McFadden, J. P., et al. (2008). THEMIS observations of a hot flow anomaly: Solar wind, magnetosheath, and ground-based measurements. *Geophysical Research Letters*, *35*, L17S03. https://doi.org/10.1029/2008GL033475

Eastwood, J. P., Sibeck, D. G., Slavin, J. A., Goldstein, M. L., Lavraud, B., Sitnov, M., et al. (2005). Observations of multiple X-line structure in the Earth's magnetotail current sheet: A Cluster case study. *Geophysical Research Letters*, *32*, L11105. https://doi.org/10.1029/2005GL022509

Ergun, R. E., Andersson, L., Peterson, W. K., Brain, D., Delory, G. T., Mitchell, D. L., et al. (2006). Role of plasma waves in Mars' atmospheric loss. *Geophysical Research Letters*, *33*, l14103. https://doi.org/10.1029/2006GL025785

Espley, J. R., Cloutier, P. A., Brain, D. A., & Crider, D. H. (2004). Observations of low-frequency magnetic oscillations in the Martian magnetosheath, magnetic pileup region, and tail. *Journal of Geophysical Research*, *109*, A07213. https://doi.org/10.1029/2003JA010193

Espley, J. R., Cloutier, P. A., Crider, D. H., Brain, D. A., & AcuÃ, M. H. (2005). Low-frequency plasma oscillations at Mars during the October 2003 solar storm. *Journal of Geophysical Research*, *110*, a09S33. https://doi.org/10.1029/2004JA010935

Espley, J. R., Delory, G. T., & Cloutier, P. A. (2006). Initial observations of low-frequency magnetic fluctuations in the Martian ionosphere. *Journal of Geophysical Research*, *111*, E06S22. https://doi.org/10.1029/2005JE002587

Fairfield, D. H. (1976). Magnetic fields of the magnetosheath. *Reviews of Geophysics and Space Physics*, *14*, 117–134. https://doi.org/10.1029/RG014i001p00117

Farrugia, C. J., Freeman, M. P., Cowley, S. W. H., Southwood, D. J., Lockwood, M., & Etemadi, A. (1989). Pressure-driven magnetopause motions and attendant response on the ground. *Planetary and Space Science*, *37*, 589–607. https://doi.org/10.1016/0032-0633(89)90099-8

Fowler, C. M., Anderson, L., Ergun, R. E., Harada, Y., Hara, T., Collinson, G., et al. (2018). MAVEN observations of solar wind driven magnetosonic waves heating the Martian dayside ionosphere. *Journal of Geophysical Research: Space Physics*, *123*, 4129–4149. https://doi.org/10.1029/2018JA025208

Fowler, C. M., Andersson, J., Halekas, J., Espley, J. R., Mazelle, C., Coughlin, E. R., et al. (2017). Electric and magnetic variations in the near-Mars environment. *Journal of Geophysical Research: Space Physics*, *122*, 8536–8559. https://doi.org/10.1002/2016JA023411

Francia, P., Regi, M., De Lauretis, M., Villante, U., & Pilipenko, V. A. (2012). A case study of upstream wave transmission to the ground at polar and low latitudes. *Journal of Geophysical Research*, *117*, A01210. https://doi.org/10.1029/2011JA016751

Fränz, M., Echer, E., Marques de Souza, A., Dubinin, E., & Zhang, T. L. (2017). Ultra low frequency waves at Venus: Observations by the Venus Express spacecraft. *Planetary and Space Science*, *146*, 55–65. https://doi.org/10.1016/j.pss.2017.08.011

Glassmeier, K.-H., Klimushkin, D., Othmer, C., & Mager, P. (2004). ULF waves at Mercury: Earth, the giants, and their little brother compared. *Advances in Space Research*, *33*, 1875–1883. https://doi.org/10.1016/j.asr.2003.04.047

Grard, R., Nairn, C., Pedersen, A., Klimov, S., Savin, S., Skalsky, A., & Trotignon, J. G. (1991). Plasma and waves around Mars. *Planetary and Space Science*, *39*, 89–93. https://doi.org/10.1016/0032-0633(91)90131-S

Greenstadt, E. W. (1986). Comparative ULF foreshocks of Earth and Venus observed by ISEE 1 and PVO. *Advances in Space Research*, *6*, 77–83. https://doi.org/10.1016/0273-1177(86)90015-3

Greenstadt, E. W., Green, I. M., Inouye, G. T., Hundhausen, A. J., Bame, S. J., & Strong, I. B. (1968). Correlated magnetic field and plasma observations of the Earth's bow shock. *Journal of Geophysical Research*, *73*, 51–60. https://doi.org/10.1029/JA073i001p00051

Halekas, J. S., McFadden, J. P., Connerny, J. E. P., Espley, J. R., Brain, D. A., Mitchell, D. L., et al. (2015). Time-dispersed ion signatures observed in the Martian magnetosphere by MAVEN. *Geophysical Research Letters*, *42*, 8910–8916. https://doi.org/10.1002/2015GL064781

Halekas, J. S., Ruhunusiri, S., Harada, Y., Collinson, G., Mitchell, D. L., Mazelle, C., et al. (2017). Structure, dynamics, and seasonal variability of the Mars-solar wind interaction: MAVEN solar wind ion analyzer in-flight performance and science results. *Journal of Geophysical Research: Space Physics*, *122*, 547–578. https://doi.org/10.1002/2016JA023167

Halekas, J. S., Taylor, E. R., Dalton, G., Johnson, G., Curtis, D. W., McFadden, J. P., et al. (2015). The solar wind ion analyzer for MAVEN. *Space Science Reviews*, *195*, 125–151. https://doi.org/10.1007/s11214-013-0029-z

Hoppe, M. M., & Russell, C. T. (1983). Plasma rest frame frequencies and polarizations of the low-frequency upstream waves—ISEE 1 and 2 observations. *Journal of Geophysical Research*, *88*, 2021–2027. https://doi.org/10.1029/JA088iA03p02021

Lichtenegger, H. I. M., Gröller, H., Lammer, H., Kulikov, Y. N., & Shematovich, V. I. (2009). On the elusive hot oxygen corona of Venus. *Geophysical Research Letters*, *36*, L10204. https://doi.org/10.1029/2009GL037575

Lucek, E. A., Horbury, T. S., Dandouras, I., & Rème, H. (2008). Cluster observations of the Earth's quasi-parallel bow shock. *Journal of Geophysical Research*, *113*, A07S02. https://doi.org/10.1029/2007JA012756

Luhmann, J. G., Russell, C. T., Phillips, J. L., & Barnes, A. (1987). On the role of the quasi-parallel bow shock in ion pickup—A lesson from Venus?*Journal of Geophysical Research*, *92*, 2544–2550. https://doi.org/10.1029/JA092iA03p02544

Luhmann, J. G., Tatrallyay, M., Russell, C. T., & Winterhalter, D. (1983). Magnetic field fluctuations in the Venus magnetosheath. *Geophysical Research Letters*, *10*, 655–658. https://doi.org/10.1029/GL010i008p00655

Lundin, R., Barabash, S., Andersson, H., Holmström M., Grigoriev, A., Yamauchi, M., et al. (2004). Solar wind-induced atmospheric erosion at Mars: First results from ASPERA-3 on Mars Express. *Science*, *305*, 1933–1936. https://doi.org/10.1126/science.1101860

Lundin, R., Barabash, S., Dubinin, E., Winningham, D., Yamauchi, M., Sauvaud, J. A., et al. (2011). Low-altitude acceleration of ionospheric ions at Mars. *Geophysical Research Letters*, *38*, l08108. https://doi.org/10.1029/2011GL047064

Mann, G., Luehr, H., & Baumjohann, W. (1994). Statistical analysis of short large-amplitude magnetic field structures in the vicinity of the quasi-parallel bow shock. *Journal of Geophysical Research*, *99*, 13,315–13,323. https://doi.org/10.1029/94JA00440

Martinecz, C., Fränz, M., Woch, J., Krupp, N., Roussos, E., Dubinin, E., et al. (2008). Location of the bow shock and ion composition boundaries at Venus—Initial determinations from Venus Express ASPERA-4. *Planetary and Space Science*, *56*, 780–784. https://doi.org/10.1016/j.pss.2007.07.007

Mazelle, C., Winterhalter, D., Winterhalter, K., Trotignon, J. G., Acuña, M. H., Baumgärtel, K., et al. (2004). Bow shock and upstream phenomena at Mars. *Space Science Reviews*, *111*, 115–181. https://doi.org/10.1023/B:SPAC.0000032717.98679.d0

McFadden, J. P., Kortmann, O., Curtis, D., Dalton, G., Johnson, J., & Abiad, R. (2015). MAVEN SupraThermal and Thermal Ion Compostion (STATIC) instrument. *Space Science Reviews*, *195*, 199–256. https://doi.org/10.1007/s11214-015-0175-6

Mitchell, D. L., Mazelle, C., Sauvaud, J.-A., Thocaven, J.-J., Rouzaud, J., Fedorov, A., et al. (2016). The MAVEN solar wind electron analyzer. *Space Science Reviews*, *200*, 495–528. https://doi.org/10.1007/s11214-015-0232-1

Ness, N. F., Behannon, K. W., Lepping, R. P., Whang, Y. C., & Schatten, K. H. (1974). Magnetic field observations near Venus: Preliminary results from Mariner 10. *Science*, *183*, 1301–1306.

Omidi, N., Collinson, G., & Sibeck, D. (2017). Structure and properties of the foreshock at Venus. *Journal of Geophysical Research: Space Physics*, *122*, 10,275–10,286. https://doi.org/10.1002/2017JA024180

Omidi, N., & Winske, D. (1990). Steepening of kinetic magnetosonic waves into shocklets—Simulations and consequences for planetary shocks and comets. *Journal of Geophysical Research*, *95*, 2281–2300. https://doi.org/10.1029/JA095iA03p02281

Orlowski, D. S., & Russell, C. T. (1991). ULF waves upstream of the Venus bow shock—Properties of one-hertz waves. *Journal of Geophysical Research*, *96*, 11,271–11,282. https://doi.org/10.1029/91JA01103

Parker, E. N. (1958). Dynamics of the interplanetary gas and magnetic fields. *Astrophysical Journal*, *128*, 664.

Parker, E. N. (1963). *Interplanetary dynamical processes* (pp. 1963). New York: Interscience Publishers.

Parker, E. N. (1965). Dynamical theory of the solar wind. *Space Science Reviews*, *4*, 666–708. https://doi.org/10.1007/BF00216273

Potapov, A. S., & Polyushkina, N. (2010). Experimental evidence for direct penetration of ULF waves from the solar wind and their possible effect on acceleration of radiation belt electrons. *Geomagnetism and Aeronomy*, *50*, 950–957. https://doi.org/10.1134/S0016793210080049

Regi, M., De Lauretis, M., Francia, P., & Villante, U. (2014). The propagation of ULF waves from the Earth's foreshock region to ground: The case study of 15 February 2009. *Earth, Planets, and Space*, *66*, 43. https://doi.org/10.1186/1880-5981-66-43

Romanelli, N., Mazelle, C., Chaufray, J. Y., Meziane, K., Shan, L., Ruhunusiri, S., et al. (2016). Proton cyclotron waves occurrence rate upstream from Mars observed by MAVEN: Associated variability of the Martian upper atmosphere. *Journal of Geophysical Research: Space Physics*, *121*, 11,113–11,128. https://doi.org/10.1002/2016JA023270

Ruhunusiri, S., Halekas, J. S., Connerney, J. E. P., Espley, J. R., McFadden, J. P., Mazelle, C., et al. (2016). MAVEN observation of an obliquely propagating low-frequency wave upstream of Mars. *Journal of Geophysical Research: Space Physics*, *121*, 2374–2389. https://doi.org/10.1002/2015JA022306

Russell, C. T., Chou, E., Gazis, P., Brace, L. H., & Hoegy, W. R. (1988). Solar and interplanetary control of the location of the Venus bow shock. *Journal of Geophysical Research*, *93*, 5461–5469. https://doi.org/10.1029/JA093iA06p05461

Russell, C. T., Elphic, R. C., & Slavin, J. A. (1979). Initial Pioneer Venus magnetic field results—Dayside observations. *Science*, *203*, 745–748.
Russell, C. T., Luhmann, J. G., Odera, T. J., & Stuart, W. F. (1983). The rate of occurrence of dayside Pc 3,4 pulsations—The L-value dependence of the IMF cone angle effect. *Geophysical Research Letters*, *10*, 663–666. https://doi.org/10.1029/GL010i008p00663
Russell, C. T., Luhmann, J. G., Schwingenschuh, K., Riedler, W., & Yeroshenko, Y. (1990). Upstream waves at Mars—PHOBOS observations. *Geophysical Research Letters*, *17*, 897–900. https://doi.org/10.1029/GL017i006p00897
Schwartz, S. J., & Burgess, D. (1991). Quasi-parallel shocks—A patchwork of three-dimensional structures. *Geophysical Research Letters*, *18*, 373–376. https://doi.org/10.1029/91GL00138
Sibeck, D. G., Baumjohann, W., & Lopez, R. E. (1989). Solar wind dynamic pressure variations and transient magnetospheric signatures. *Geophysical Research Letters*, *16*, 13–16. https://doi.org/10.1029/GL016i001p00013
Sibeck, D. G., Borodkova, N. L., Schwartz, S. J., Owen, C. J., Kessel, R., Kokubun, S., et al. (1999). Comprehensive study of the magnetospheric response to a hot flow anomaly. *Journal of Geophysical Research*, *104*, 4577–4594. https://doi.org/10.1029/1998JA900021
Sibeck, D. G., Borodkova, N. L., Zastenker, G. N., Romanov, S. A., & Sauvaud, J.-A. (1998). Gross deformation of the dayside magnetopause. *Geophysical Research Letters*, *25*, 453–456. https://doi.org/10.1029/98GL00134
Slavin, J. A., Acuña, M. H., Anderson, B. J., Barabash, S., Benna, M., Boardsen, S. A., et al. (2009). MESSENGER and Venus Express observations of the solar wind interaction with Venus. *Geophysical Research Letters*, *36*, 106. https://doi.org/10.1029/2009GL037876
Strangeway, R. J. (1991). Polarization of the impulsive signals observed in the nightside ionosphere of Venus. *Journal of Geophysical Research*, *96*(E5), 22741–22752. https://doi.org/10.1029/91JE02506
Strangeway, R. J. (2004). Plasma waves and electromagnetic radiation at Venus and Mars. *Advances in Space Research*, *33*, 1956–1967. https://doi.org/10.1016/j.asr.2003.08.040
Torrence, C., & Compo, G. P. (1998). A practical guide to wavelet analysis. *Bulletin of the American Meteorological Society*, *79*, 61–78. https://doi.org/10.1175/1520-0477(1998)079
Tsubouchi, K., & Lembège, B. (2004). Full particle simulations of short large-amplitude magnetic structures (SLAMS) in quasi-parallel shocks. *Journal of Geophysical Research*, *109*, A02114. https://doi.org/10.1029/2003JA010014
Vignes, D., Mazelle, C., Rme, H., Acuña, M. H., Connerne, J. E. P., Lin, R. P., et al. (2000). The solar wind interaction with Mars: Locations and shapes of the bow shock and the magnetic pile-up boundary from the observations of the MAG/ER Experiment onboard Mars Global Surveyor. *Geophysical Research Letters*, *27*, 49–52. https://doi.org/10.1029/1999GL010703
Villante, U., De Paulis, C., & Francia, P. (2011). The transmission of upstream waves to the magnetosphere: An analysis at widely separated ground stations. *Journal of Geophysical Research*, *116*, A06219. https://doi.org/10.1029/2010JA016263
Wei, H. Y., Russell, C. T., Zhang, T. L., & Blanco-Cano, X. (2011). Comparative study of ion cyclotron waves at Mars, Venus and Earth. *Planetary and Space Science*, *59*, 1039–1047. https://doi.org/10.1016/j.pss.2010.01.004
Wilson, L. B. III (2016). Low frequency waves at and upstream of collisionless shocks. *Washington DC American Geophysical Union Geophysical Monograph Series*, *216*, 269–291. https://doi.org/10.1002/9781119055006.ch16
Wilson, L. B. III, Cattell, C. A., Kellogg, P. J., Goetz, K., Kersten, K., Kasper, J. C., et al. (2009). Low-frequency whistler waves and shocklets observed at quasi-perpendicular interplanetary shocks. *Journal of Geophysical Research*, *114*, A10106. https://doi.org/10.1029/2009JA014376
Winningham, J. D., Frahm, R. A., Sharber, J. R., Coates, A. J., Linder, D. R., Soobiah, Y., et al. (2006). Electron oscillations in the induced Martian magnetosphere. *Icarus*, *182*, 360–370. https://doi.org/10.1016/j.icarus.2005.10.033 Results from the Mars Express ASPERA-3 Investigation.
Yamauchi, M., Hara, T., Lundin, R., Dubinin, E., Fedorov, A., Sauvaud, J.-A., et al. (2015). Seasonal variation of Martian pick-up ions: Evidence of breathing exosphere. *Planetary and Space Science*, *119*, 54–61. https://doi.org/10.1016/j.pss.2015.09.013